Journal of Magnetic Resonance 200 (2009) 101–108

Contents lists available at ScienceDirect

Journal of Magnetic Resonance

journal homepage: www.elsevier.com/locate/jmr

Visualization of enantiomers using natural abundant ^{13}C-filtered single and double quantum selective refocusing experiments: Application to small chiral molecules

Nilamoni Nath [a,b], Bikash Baishya [a,1], N. Suryaprakash [a,*]

[a] NMR Research Centre, Indian Institute of Science, Bangalore 560012, India
[b] Solid State and Structural Chemistry Unit, Indian Institute of Science, Bangalore 560012, India

ARTICLE INFO

Article history:
Received 18 March 2009
Revised 9 May 2009
Available online 17 June 2009

Keywords:
Chiral discrimination
Double quantum
Selective excitation
DQSERF
CH-SERF
CH-DQSERF
Dipolar couplings

ABSTRACT

The routine use of proton NMR for the visualization of enantiomers, aligned in the chiral liquid crystal solvent poly-γ-benzyl-L-glutamate (PBLG), is restricted due to severe loss of resolution arising from large number of pair wise interaction of nuclear spins. In the present study, we have designed two experimental techniques for their visualization utilizing the natural abundance ^{13}C edited selective refocusing of single quantum (CH-SERF) and double quantum (CH-DQSERF) coherences. The methods achieve chiral discrimination and aid in the simultaneous determination of homonuclear couplings between active and passive spins and heteronuclear couplings between the excited protons and the participating ^{13}C spin. The CH-SERF also overcomes the problem of overlap of central transitions of the methyl selective refocusing (SERF) experiment resulting in better chiral discrimination. Theoretical description of the evolution of magnetization in both the sequences has been discussed using polarization operator formalism.

1. Introduction

The design and synthesis of optically pure compounds are the two challenges in modern organic chemistry and biochemistry. In achieving this goal the chiral discrimination and the determination of enantiomeric excess are of profound importance. Several aligning media, viz., collagen fibers, stretched gelatin gels, chiral cages, cholesteric phases, polyamino acids have been reported for discrimination of enantiomers [1–6]. The large part of the work in the literature, however, employs the chiral liquid crystal poly-γ-benzyl-L-glutamate (PBLG) as an aligning medium [7–10]. Recently, the use of liquid crystalline phase of fragmented DNA solution has been demonstrated as an alternate orienting medium [11]. The commonly encountered NMR active nuclei for the investigation of chiral molecules are ^{1}H, natural abundant ^{13}C and ^{2}H. In the aligned medium there will be a differential ordering effect on the NMR parameters of these nuclei, viz., chemical shift anisotropies ($\Delta\sigma_i$), dipolar couplings (D_{ij}) and quadrupolar couplings (Q_i). Distinctly different values of these parameters enable the visualization of enantiomers. The strengths of ^{2}H quadrupole couplings are relatively larger compared to $\Delta\sigma_{1H}$, $\Delta\sigma_{13C}$, D_{CH} and D_{HH}. Thus, large part of the reported work is focused on ^{2}H NMR studies [12–19]. A recent review provides the latest account of the literature on the use of natural abundant deuterium NMR [20].

While the proton NMR spectroscopy has the advantage of high sensitivity, the ^{1}H NMR spectra of chiral molecules become rapidly complex with increase in the number of interacting spins due to large number of short and long distance dipolar couplings. There is also severe loss of resolution arising from too many degenerate transitions, in addition to the superposition of the spectra from both the enantiomers. The basic requirement for the analyses of such spectra is the enantiodiscrimination and the discerning of the overlapped transitions. This is a formidable task even for small molecules with five or six interacting spins. Thus, the present methodologies are applicable to small molecules. In spite of all these difficulties there are several methods developed for visualization of enantiomers by ^{1}H NMR. A brief review summarizes the available proton NMR experiments [21]. A recent work reports the application of chemical shift resolved 2D experiment for visualization of enantiomers [22]. Several experimental techniques are reported not only for the enantiodiscrimination but also for the simplification of the complex ^{1}H NMR spectra and to derive the spectral parameters [23–29]. In this study, we report two experimental schemes designed for discrimination and analyses of ^{13}C-filtered ^{1}H NMR spectra of molecules aligned in the chiral liquid crystal PBLG solvent.

The present work is on the development of reported SERF [30,31] and double quantum selective refocusing (DQ-SERF) exper-

* Corresponding author. Fax: +91 80 2360 1550.
E-mail address: nsp@sif.iisc.ernet.in (N. Suryaprakash).
[1] Present address: Ecole Polytechnique Fédérale de Lausanne, Switzerland.

1090-7807/$ - see front matter © 2009 Elsevier Inc. All rights reserved.
doi:10.1016/j.jmr.2009.06.011

iments [23] utilizing INEPT (Insensitive Nuclei Enhanced by Polarization Transfer) [32] for enhancing the signal intensity. The use of INEPT sequence for the visualization of enantiomers has been demonstrated in heteronuclear correlation experiments [3,33]. The present methods apply INEPT for two-dimensional resolved experiments. The pulse sequences are the blend of INEPT with two-dimensional spin selective single quantum (SQ) and double quantum (DQ) coherences and are designated as CH-SERF and CH-DQSERF, respectively. The designed experiments aid in chiral discrimination and the simultaneous determination of homonuclear (D_{HH}) and heteronuclear (D_{CH}) couplings. The techniques are demonstrated on different chiral molecules.

2. Experimental investigation

For the experimental demonstration of the designed pulse sequences three molecules, viz., (*R/S*)-2-chloropropanoic acid (**1**), (*R/S*)-3-butyn-2-ol (**2**) and (*R/S*)-propylene carbonate (**3**) have been chosen. These molecules are chosen as they are different types of spin systems and aid in better understanding of the spin dynamics in the present sequences. The aligned samples were prepared by the method reported in the literature [29,34]. For the oriented sample **1**, 80 mg of PBLG, 50 mg of **1** and 300 mg of $CDCl_3$ were taken. For the oriented sample **2** and **3**, respectively, 85 and 102.8 mg of PBLG, 59 and 53 mg of solute and 450 and 665 mg of $CDCl_3$ were taken. The one- and two-dimensional spectra of all the molecules were recorded using Bruker DRX-500 NMR spectrometer. The temperature was maintained at 300 K for all the samples, using Bruker BVT 3000 temperature controller unit. The alignment of each sample was confirmed by monitoring the ^2H doublet separation of $CDCl_3$. The CH-SERF and CH-DQSERF pulse sequences, the racemic structures of the investigated molecules are given in Fig. 1. The assignment of peaks for enantiomers *R* and *S* is generally carried out by initially recording the spectrum of enantiopure sample and comparing it with the spectrum of a racemic mixture. The one-dimensional proton spectra and the assignment of peaks for different protons and for enantiomers *R* and *S* have already been discussed earlier [24,26]. Hence, we choose to provide the one-dimensional spectra as Supplementary Material. For all the molecules our earlier reported assignments for *R* and *S* enantiomers have been retained [25]. The acquisition and processing parameters for CH-SERF and CH-DQSERF experiments are summarized in Table 1. For all the experiments the SEDUCE shaped selective pulses were utilized and their durations are reported in the respective figure captions and the table. The 90° and 180° pulses of identical durations were calibrated with different rf power. All experimental parameters are given in the respective figure captions.

2.1. Evolution of magnetization in the pulse sequences

The polarization operator formalism [35] is employed for understanding the spin dynamics and appearance of the two-dimensional spectra in CH-SERF and CH-DQSERF pulse sequences. For discussion a weakly dipolar coupled spin system of the type A_3MX (A and M are proton spins and X is a carbon spin) is chosen. Spectrum of such a spin system is influenced by two types of homonuclear couplings, $^2T_{AA}$ and $^3T_{AM}$ and one heteronuclear coupling $^1T_{AX}$ (where $T_{ij} = J_{ij} + 2D_{ij}$ for non-equivalent spins and $T_{ij} = 3\text{-}D_{ij}$ for equivalent spins and the superscript pertains to the coupled proton that is separated by that many bonds). $^2T_{MX}$ is not detected since the selective pulses are applied only on A_3 spins.

The CH-SERF pulse sequence (Fig. 1A) starts with a non-selective INEPT from ^1H to ^{13}C spin resulting in a term $I_z^A S_y^X$ (where *I* is proton and *S* is carbon) after the first hard $(\pi/2)_x$ pulse on ^{13}C.

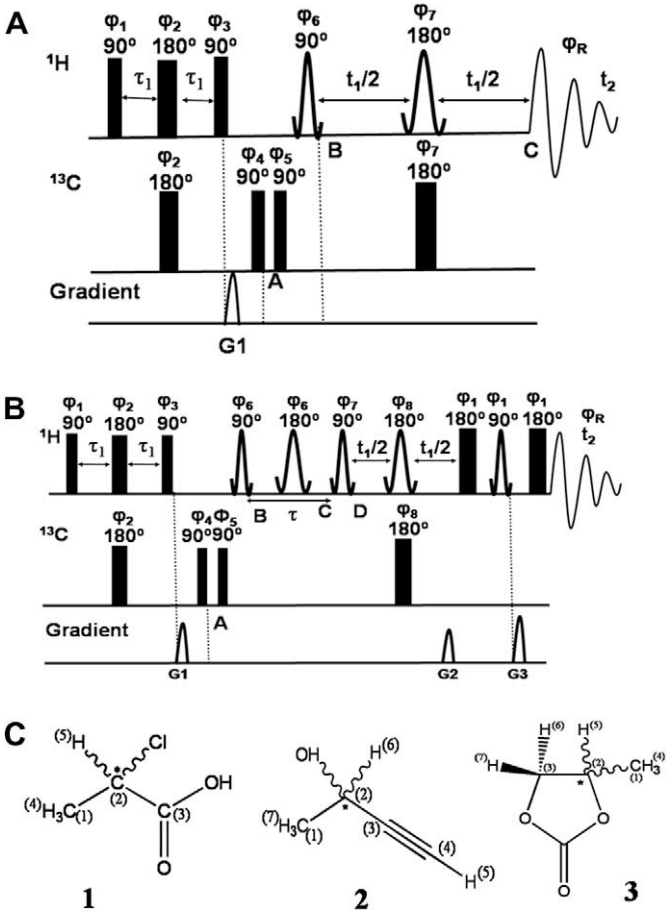

Fig. 1. (A) The pulse sequence employed for CH-SERF experiment. The behavior of the magnetization during different stages of pulse sequences is discussed in the text. Rectangular pulses are hard pulses. All the remaining pulses are spin selective. The phases of the pulses are: $\varphi_1 = x$, $\varphi_2 = x\,x\,-x\,-x$, $\varphi_3 = y$, $\varphi_4 = 4(x)\,4(-x)$, $\varphi_5 = x\,-x$, $\varphi_6 = \varphi_7 = 8(x)\,8(-x)$ and $\varphi_R = 2(x\,-x)\,4(-x\,x)\,2(x\,-x)$. (B) The pulse sequence for CH-DQSERF experiment. The phases of the pulses are $\varphi_1 = x$, $\varphi_2 = 4(x)\,4(-x)$, $\varphi_3 = y$, $\varphi_4 = 8(x)\,8(-x)$, $\varphi_5 = 4(x\,-x)$, $\varphi_6 = \varphi_7 = (8)x$, $\varphi_8 = 2(x)\,2(y)\,2(-x)\,2(-y)$, $\varphi_R = 4(x\,-x)\,4(-x\,x)$. The delay τ_1 responsible for the polarization transfer depends on the factor $1/(4(^1T_{AX}))$ and was adjusted for each molecule independently, the gradient ratio used was G2:G3 = 1:2, and (C) The racemic structure and the numbering of the interacting spins in the molecules; (*R/S*)-2-chloropropanoic acid (**1**), (*R/S*)-3-butyn-2-ol (**2**) and (*R/S*)-propylene carbonate (**3**).

The gradient employed after the second $(\pi/2)_y$ pulse on I spin suppresses the proton magnetization attached to ^{12}C. The magnetization transfer pathway during the second half (during A to B) of the pulse sequence can then be described as

$$I_z^A S_y^X \overset{(\pi/2)_x^X}{\rightarrow} I_z^A S_z^X \overset{(\pi/2)_x^A}{\rightarrow} I_y^A S_z^X \tag{1}$$

The INEPT transfer enables the spin state selection by ^{13}C. This followed by the selective excitation of A spin single quantum coherence leads to $I_y^A S_z^X$ term at the time point B. From the stage B to C, the magnetization evolves under $^2T_{AA}$ and $^1T_{AX}$ couplings due to selective 180° pulse on A_3 and a hard 180° pulse on *X* in the middle of t_1 dimension. Thus the polarization operator (i.e., $I_y^A E^A E^A S_z^X$) that evolves during the t_1 period is

$$\frac{1}{8}\left(I_+^A\right)\left[\left(I_\alpha^A + I_\beta^A\right)\right]\left[\left(I_\alpha^A + I_\beta^A\right)\right]\left(S_\alpha^X - S_\beta^X\right) \tag{2}$$

The resulting spectrum in the t_1 dimension will be doublet of a triplet arising from the dipolar couplings between A_3 spins and the states $|\alpha\rangle$ and $|\beta\rangle$ of ^{13}C spin, respectively. The absence of mixing pulse leaves the spin states of both ^1H and ^{13}C unperturbed in both

Table 1
Acquisition and processing parameters of the two-dimensional selective methyl protons excited CH-SERF and CH-DQSERF experiments in (*R*/*S*)-2-chloropropanoic acid, (*R*/*S*)-3-butyn-2-ol and (*R*/*S*)-propylene carbonate aligned in chiral liquid crystal PBLG.

Parameter	(*R*/*S*)-2-chloropropanoic acid				(*R*/*S*)-3-butyn-2-ol		(*R*/*S*)-propylene carbonate			
	CH-SERF Dimension		CH-DQSERF Dimension		CH-DQSERF Dimension		CH-SERF Dimension		CH-DQSERF Dimension	
	F_1	F_2	F_1	F_2	F_1	F_2	F_1	F_2	F_1	F_2
Spectral width (Hz)	300	300	300	400	500	600	300	300	420	280
Number of data points	148	660	304	1228	256	1800	148	660	300	700
Digital resolution (Hz)	0.29	1.17	0.98	0.32	1.56	0.38	0.29	0.48	1.04	0.25
Zero filling of data	4k	2k	1k	2k	4k	4k	4k	2k	4k	2k
Window function used	Sine	Sine	Sine	Sine	Sine	Sine	Sine	Sine	Sine	Sine
SEDUCE shaped pulse length (ms)	1.66 for both $\pi/2$ and π		1.66 for both $\pi/2$ and π		6.25 for both $\pi/2$ and π		1.66 for both $\pi/2$ and π		1.66 for both $\pi/2$ and π	
Optimized τ delay (ms)	–		20		0.69		–		3.12	
Relaxation delay (s)	2.5		2.5		2		2.5		3	
Number of accumulations	16		16		16		16		16	

t_1 and t_2 dimensions. During the t_1 period, the coupling $^3T_{AM}$ is refocused and is retained during the t_2 period. The polarization operator during the t_2 period will then be

$$\frac{1}{16}\left(I_+^A\right)\left[\left(I_\alpha^A+I_\beta^A\right)\right]\left[\left(I_\alpha^A+I_\beta^A\right)\right]\left(I_\alpha^M+I_\beta^M\right)\left(S_\alpha^X-S_\beta^X\right) \tag{3}$$

The spectrum is, therefore, a doublet of doublet of a triplet in the t_2 dimension. These six transitions appear as doublets along t_2 dimension corresponding to six states of A_3X spins.

The discussion for CH-DQSERF pulse sequence (Fig. 1B) is identical to that of sequence shown in Fig. 1A up to the point B. During the pathway from B to D, the magnetization evolves under $^2T_{AA}$ coupling since the selective 180° pulse decouples A_3 from both M and X spins and the second selective 90° pulse between time points C and D creates double quantum $I_y^A I_y^A I_z^A S_z^X$ coherence at the point D. The polarization operator during the t_1 period is

$$\frac{1}{4}\left(I_+^A I_+^A - I_+^A I_-^A - I_-^A I_+^A + I_-^A I_-^A\right)\left(I_\alpha^A+I_\beta^A\right)\left(S_\alpha^X-S_\beta^X\right) \tag{4}$$

The hard 180° pulse on ^{13}C and the selective 180° pulse on A_3 in the middle of t_1 dimension ensure the evolution of double quantum $(I_+^A I_+^A)(I_\alpha^A+I_\beta^A)(S_\alpha^X-S_\beta^X)$ term under $^2T_{AA}$ and $^1T_{CH}$ couplings. The frequency gets modulated in the t_1 dimension as

$$\exp[+i(2\Omega_A-\pi k_1-\pi k_2)t_1]+\exp[+i(2\Omega_A+\pi k_1-\pi k_2)t_1] - \exp[+i(2\Omega_A-\pi k_1+\pi k_2)t_1]-\exp[+i(2\Omega_A+\pi k_1+\pi k_2)t_1] \tag{5}$$

where $k_1 = {}^2T_{AA} + {}^2T_{AA}$ and $k_2 = {}^1T_{AX} + {}^1T_{AX}$

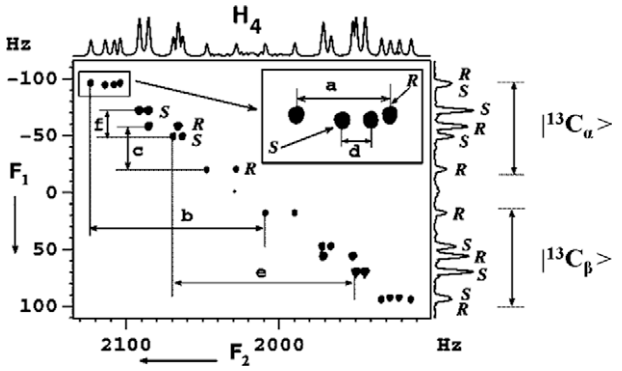

Fig. 2. The 500 MHz CH-SERF spectrum of (*R*/*S*)-2-chloropropanoic acid in PBLG. The spectrum is displayed in magnitude mode with a digital resolution of 0.29 Hz and 1.17 Hz in the direct and indirect dimensions, respectively. The optimized τ_1 delay is 1.66 ms. $|^{13}C_\alpha\rangle$ and $|^{13}C_\beta\rangle$ regions are marked in the F_1 dimension. The peaks for *R* and *S* enantiomers are labeled. The expansion of a small region of the spectrum given in the inset depicts the resolution of closely resonating transitions. The magnitudes of the couplings (in Hz) are: a = $(^3T_{HH})^R$ = 19.3, b = $(^1T_{CH})^R$ = 113.0, c = $(^2T_{HH})^R$ = 37.2 and d = $(^3T_{HH})^S$ = 6.2, e = $(^1T_{CH})^S$ = 142.0 and f = $(^2T_{HH})^S$ = 22.3.

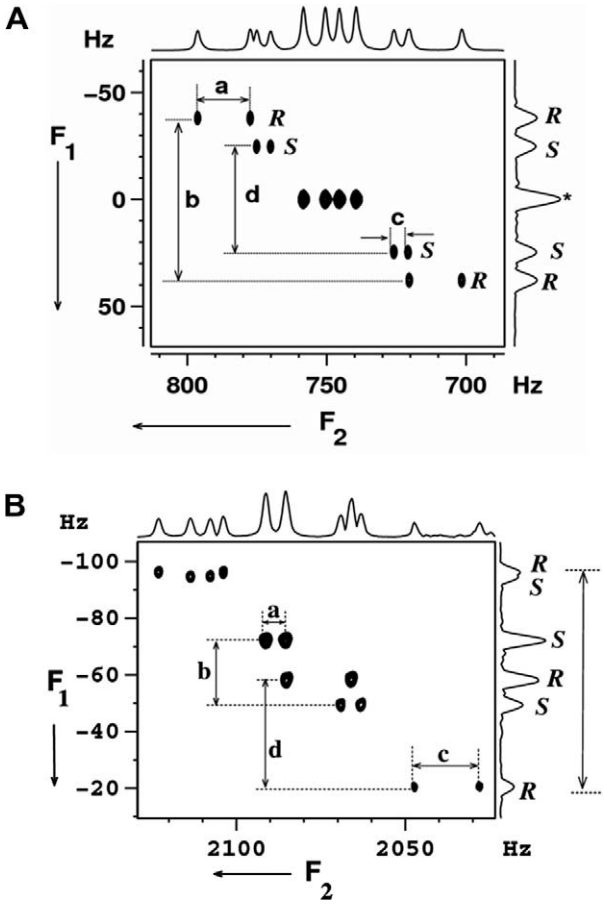

Fig. 3. (A) ^{12}C attached selective methyl group excited 2D SERF spectrum of (*R*/*S*)-2-chloropropanoic acid along with the corresponding projections. The SEDUCE shaped pulse lengths are 2.5 ms for both 90° and 180° selective pulses with rf power optimized accordingly. The size of the 2D data matrix is 700 × 128 and zero filled to 1 k in both the dimensions before processing. The peaks for *R* and *S* enantiomers are labeled. The sine bell window function is used in both the dimensions. *Marks indicate the overlap of two transitions from *R* and *S*. The magnitudes of the couplings (in Hz) are: a = $(^3T_{HH})^R$ = 19.3, b = $2(^2T_{HH})^R$ = 74.4, c = $(^3T_{HH})^S$ = 6.2 and d = $2(^2T_{HH})^S$ = 44.6 and (B) The Expanded $|^{13}C_\alpha\rangle$ region of Fig. 2 given for comparison.

The spectrum in t_1 dimension will then be a doublet of a doublet, which is in phase with respect to sum of passive homonuclear couplings (k_1) and antiphase with respect to the sum of passive heteronuclear couplings (k_2). The last selective $(\pi/2)_X$ pulse on A_3 spins converts double quantum term to the single quantum term. Since $^3T_{AM}$ is present in t_2 dimension the polarization operator terms after spin selective DQ–SQ conversion corresponding to $|\alpha\rangle$ spin state of passive spin A are:

$$\frac{1}{4i}\left(I_+^A I_+^A\right)\left(I_\alpha^A\right)\left(S_\alpha^X - S_\beta^X\right) \rightarrow \frac{1}{8}\left(I_-^A\right)\left[i\left(I_\alpha^A - I_\beta^A\right)\right]\left(I_\alpha^A + I_\beta^A\right)\left(I_\alpha^M + I_\beta^M\right)\left(S_\alpha^X - S_\beta^X\right) \quad (6)$$

[t_1 dimension] [t_2 dimension]

Thus, the spectrum in the t_2 dimension will be doublet of doublet of a triplet.

2.2. Analyses of CH-SERF spectra of (R/S)-2-chloropropanoic acid

The protons and carbon of the methyl group of this molecule form a weakly coupled spin system of the type A_3MX where A_3 corresponds to methyl protons and M is the methine proton and X is the ^{13}C coupled to methyl protons. The first order analysis of the spectrum is straightforward [25] and the theoretical treatment given in the preceding section is applicable. Since the pulse scheme involves a non-selective INEPT transfer of magnetization from ^1H to ^{13}C and then back transfer to proton, the ^{13}C edited proton magnetization is subsequently employed for selective refocusing. In the middle of the t_1 dimension, the simultaneous application of a selective refocusing π pulse on the methyl protons and a non-selective π pulse on ^{13}C retains $^1T_{CH}$ and $^2T_{HH}$ couplings of the methyl group and refocuses all the remote $^3T_{HH}$ couplings. This enhances the resolution in the t_1 dimension.

The selective methyl protons excited 2D CH-SERF spectrum of this molecule is reported in Fig. 2 with corresponding projections. This renders the spin system in the t_1 dimension to be A_3X. The magnitude of $^1T_{CH}$ being larger than $^2T_{HH}$, a triplet of a doublet is detected in the t_1 dimension. The two such distinct triplets of doublets discriminates *R* and *S* enantiomers unambiguously. The analysis of the spectrum provides $^nT_{ij}$, where the superscript *n* refers to interacting spins *i* and *j* that are *n* bonds away. The separation between the adjacent transitions of the triplet provides $^2T_{HH}$ ($3D_{HH}$). This is marked as c and f in the figure for *R* and *S* enantiomers, respectively. The spectrum in the direct dimension corresponds to the spin system of the type A_3MX, which is a doublet of doublet of a triplet. The methyl protons in the direct dimension experience three different couplings, viz., among themselves ($^2T_{HH}$), to methine proton ($^3T_{HH}$) and to ^{13}C of methyl group ($^1T_{CH}$). The correlated peaks appear tilted due to the presence of $^2T_{HH}$ and $^1T_{CH}$ in both the dimensions. The cross-section taken parallel to the t_2 dimension provides $(^3T_{HH})^{R/S}$. The analysis of the spectrum corresponding to either $|^{13}C_\alpha\rangle$ or $|^{13}C_\beta\rangle$ spin states provides all homonuclear couplings. The separations marked a and c in Fig. 2 provide $^3T_{HH}$ and $^2T_{HH}$, respectively, for *R* enantiomer. The corresponding parameters for *S* enantiomer are marked d and f, respectively. The displacement between two cross-sections of $|^{13}C_\alpha\rangle$ and $|^{13}C_\beta\rangle$ spin states provides $(^1T_{CH})^{R/S}$ and are marked b and e, respectively.

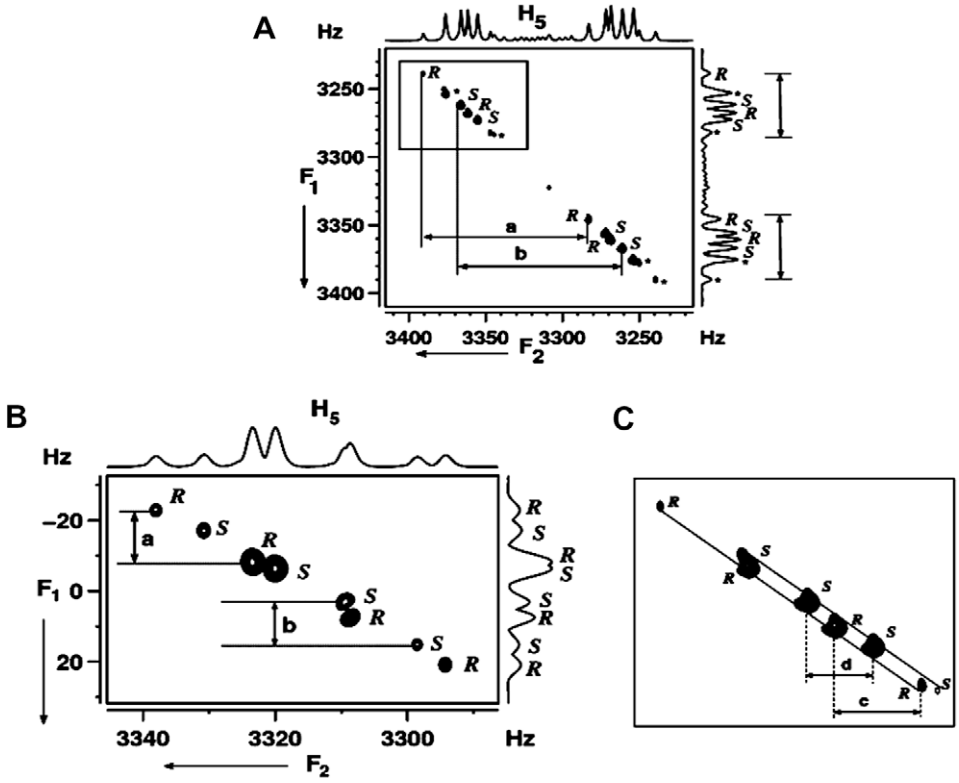

Fig. 4. (A) The 500 MHz methine proton (H5) excited CH-SERF spectrum of **1** in PBLG. The optimized τ delay is 2.08 ms. The SEDUCE shaped pulse lengths are 7.14 ms for 90° and 180° selective pulses with rf power optimized accordingly. The 2D data matrix is 720 and 164 points in F_2 and F_1 dimensions, respectively. Spectral widths of 200 and 190 Hz were chosen in the direct and indirect dimensions, respectively. The number of accumulations was 32 for each t_1 increment. Relaxation delay used was 2.5 s. The time domain data was processed by zero filling it to 2k and 1k points in F_2 and F_1 dimensions, respectively, with sine square bell window function and without linear prediction. The spectrum was displayed in magnitude mode with a digital resolution of 0.29 and 0.48 Hz in the direct and indirect dimensions, respectively. $|^{13}C_\alpha\rangle$ (bottom portion shown with double headed arrow) and $|^{13}C_\beta\rangle$ (top portion shown with double headed arrow) regions are marked in the F_1 dimension. (B) ^{12}C detected 500 MHz methine proton (H5) excited SERF spectrum of **1** in PBLG. (C) The expanded region of Fig. 4A depicted in rectangle. The quartet peaks for each enantiomer is marked with a tilted line joining the peaks. The separations providing the magnitudes of the couplings and their values (in Hz) are: a = $(^1T_{CH})^R$ = 107.7, b = $(^1T_{CH})^S$ = 104.5, c = $(^3T_{HH})^R$ = 14.4 and d = $(^3T_{HH})^S$ = 10.8.

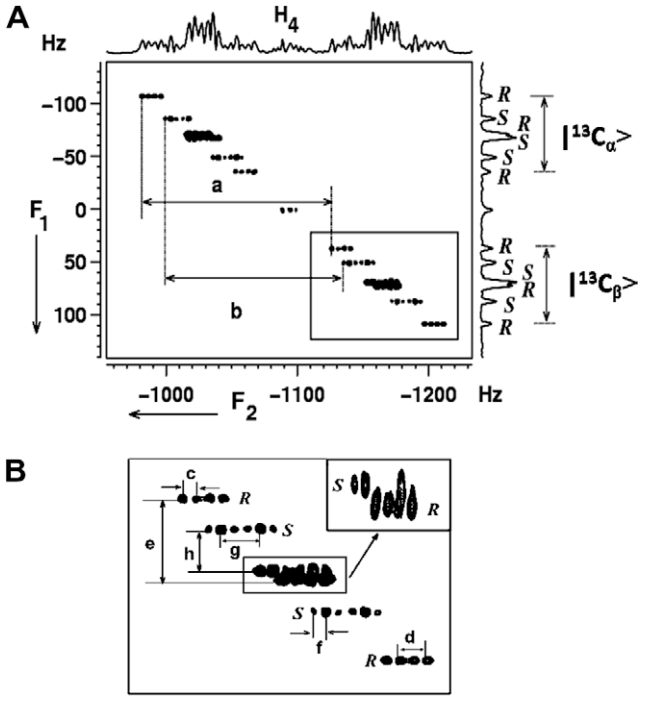

Fig. 5. The 500 MHz CH-SERF spectrum of (*R*/*S*)-propylene carbonate in PBLG. The spectrum is displayed in magnitude mode. The optimized τ_1 delay is 1.72 ms. $|\alpha(^{13}C)\rangle$ and $|\beta(^{13}C)\rangle$ regions are marked in the F_1 dimension. (B) The expanded region of Fig. 5A shown in solid rectangle. Further expansion is given in the inset for depicting the total enantio discrimination. The magnitudes of the coupling parameters (in Hz) are: a = $(^1T_{CH})^R$ = 144.0, c = $(^4T_{HH})^R$ = 4.8, d = $(^3T_{HH})^R$ = 13.7, e = $(^2T_{HH})^R$ = 50.2 and b = $(^1T_{CH})^S$ = 136.0, f = $(^4T_{HH})^S$ = 4.5, g = $(^3T_{HH})^S$ = 9.8, h = $(^2T_{HH})^S$ = 18.0.

The conventional two-dimensional SERF spectrum is reported in Fig. 3A. Though $^2T_{HH}$ are different for the enantiomers, the central peaks of the two triplets resonating at the zero frequency are overlapped due to negligible difference in their chemical shift anisotropies. In the CH-SERF experiment, as a consequence of the introduction of $^1T_{CH}$ as an additional parameter with their significantly different values, there is complete discrimination of enantiomers. This is evident from comparison of the $|^{13}C_\alpha\rangle$ region of the CH-SERF and conventional SERF spectra reported in Fig. 3B.

The CH-SERF experiment was also carried out on methine proton. The application of a biselective 180° pulse on methine and methyl protons enabled the evolution of its magnetization under $^3T_{HH}$ coupling. The corresponding CH-SERF and SERF spectra are reported in Fig. 4A and B, respectively. The evolution of $^3T_{HH}$ and $^1T_{CH}$ in the F_1 dimension results in a quartet of a doublet for each enantiomer. Each component of the doublet with larger separation ($^1T_{CH}$) is further split into a quartet ($^3T_{HH}$). The complete discrimination is evident from the tilted broken line joining the four transitions of each enantiomer reported in Fig. 4C.

2.3. Analyses of CH-SERF spectra of (R/S)-propylene carbonate

The pulse sequence was applied for the molecule **3** whose ^{1}H spectrum is more complex compared to that of molecule **1**. The spin system for this molecule would be A_3MPKX, where X is ^{13}C spin coupled to methyl protons and the remaining spins are protons. The analysis of the proton spectrum of this molecule has already been discussed [23–25]. The selective methyl protons excited CH-SERF spectrum is reported in Fig. 5A along with the F_1 and F_2 projections. The spin system in the t_1 dimension mimics A_3X type where A and X designate methyl protons and ^{13}C coupled to it, respectively. Because of larger value of $^1T_{CH}$ compared to $^2T_{HH}$ distinct triplet of a doublet is detected in t_1 dimension for each enantiomer, resulting in their discrimination. The separations marked e and h in Fig. 5B provide $^2T_{HH}$ for *R* and *S*, respectively. The methyl protons in the direct dimension pertain to A_3 part of A_3MNPX type, the analysis of which provides $^2T_{HH}$, $^3T_{HH}$, $^4T_{HH}$ and $^1T_{CH}$ for both *R* and *S* enantiomers. The couplings $^3T_{HH}$ and $^4T_{HH}$ appear only in the cross-sections taken parallel to t_2 dimension. The

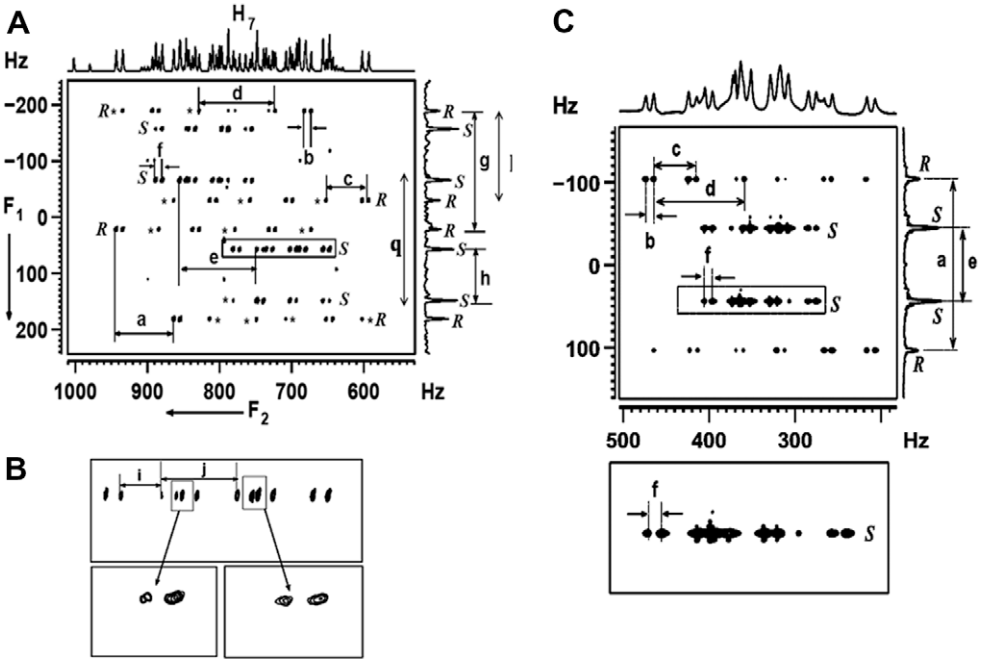

Fig. 6. (A) 500 MHz ^{1}H 2D CH-DQSERF spectrum of **2** in the chiral liquid crystal PBLG along with F_1 and F_2 projections. The optimized τ_1 delay is 1.92 ms. Peak separations providing the values of $^2T_{HH}$ ($3\times$ $^2D_{HH}$), $^3T_{HH}$ for *R* and *S* are marked. All the peaks of 2D projection in the direct dimension could be correlated to the peaks in *R* and *S* enantiomer cross-sections. Peaks marked * are of low intensity [23] and can be seen in the magnified scale. (B) Expanded region of a narrow strip marked with broken rectangle corresponding to *S* enantiomer and (C) the 500 MHz ^{1}H 2D DQSERF spectrum of **2** in the chiral liquid crystal PBLG along with F_1 and F_2 projections. A cross-section for *S* enantiomer is expanded in the box below. The values of the parameters (in Hz) are: a = $(^1T_{CH})^R$ = 78.4, g = $2(^2T_{HH})^R$ = 210.4, b = $(^5T_{HH})^R$ = 9.8, c = $(^3T_{HH})^R$ = 36.1, d = $(^2T_{HH})^R$ =105.2 Hz, e = $(^1T_{CH})^S$ = 106.5, h = $2(^2T_{HH})^S$ = 93.8, f = $(^5T_{HH})^S$ = 8.9, j = $(^2T_{HH})^S$ = 46.9 and i = $(^3T_{HH})^S$ = 36.1, l = $2(^1T_{CH})^R$ = 156.8 and q = $2(^1T_{CH})^S$ = 213.0.

separations marked a, c and d provide $^{1}T_{CH}$, $^{4}T_{HH}$ and $^{3}T_{HH}$, respectively, for *R* enantiomer and the separations b, f and g provide these parameters for *S* enantiomer. One of the remote couplings could not be determined for *R* enantiomer because of its negligible magnitude and are hidden within the line width while two different $^{4}T_{HH}$ couplings for *S* being equal, a triplet is detected. The separations providing the parameters and their magnitudes (signs are not determined) for all the investigated molecules are reported in the corresponding figure captions.

2.4. Analyses of CH-DQSERF spectra of (R/S)-3-butyn-2-ol

For the experimental demonstration of CH-DQSERF we chose molecule **2** whose spin system and ^{1}H spectrum is more complex compared to molecule **1**. The one-dimensional spectrum of **2** in the chiral liquid crystal PBLG has well isolated peaks for all the groups of protons. With the inclusion of the ^{13}C spin coupled to methyl protons, the spin system of this molecule corresponds to A_3MPX. The pulse sequence given in Fig. 1B was employed for CH-DQSERF experiment. The selectively methyl group excited CH-DQSERF spectrum is given in Fig. 6A. The spin system A_3X in the t_1 dimension mimics an AMX type where A is a super spin composed of two protons (active spins) taking part in DQ coherence and M is a passive proton not involved in the DQ coherence and X is the ^{13}C spin coupled to methyl protons. A part of AMX is detected in the DQ dimension. Thus the multiplicity pattern in the t_1 dimension is a doublet of a doublet for each enantiomer corresponding to four possible spin states of M and X. The doublet separations marked 'g' and 'h' corresponds to the sum of passive couplings $2(^{2}T_{HH})$ for *R* and *S* enantiomers, respectively. Similarly the doublet separations marked 'q' and 'l' corresponds to the sum of passive couplings $2(^{1}T_{CH})$ for *R* and *S* enantiomers, respectively. Interestingly in this specific example $^{1}T_{CH}$ is smaller than $^{2}T_{HH}$, hence there is no isolated groups of transitions pertaining to spin states $|\alpha\rangle$ and $|\beta\rangle$ of ^{13}C, unlike in CH-SERF spectra of the molecules discussed previously.

In the direct dimension spin system corresponds to A_3MPX and displays all the couplings. The spectral pattern for the CH-DQSERF experiment appears different from CH-SERF experiment. This is the consequence of the DQ excitation in the preparation period and the presence of the mixing pulse (i.e. DQ–SQ conversion pulse) at the end of t_1 dimension. The SQ cross-section for each transition in the DQ dimension gives rise to enantiopure proton spectrum edited by ^{13}C spin of the methyl group. The cross-section for *R* and *S* enantiomers provides the parameters, $^{2}T_{HH}$, $^{3}T_{HH}$, $^{5}T_{HH}$. The $^{1}T_{CH}$ appears as a displacement between the two cross-sections. Thus all the couplings experienced by methyl protons could be extracted from the direct dimension. For comparison, DQSERF spectrum of **2** is given in Fig. 6C. From the t_2 dimension of this spectrum only one coupling is derivable for the *S* enantiomer. As a result of routing the magnetization through ^{13}C and invoking $^{1}T_{CH}$ in CH-DQSERF, all the three couplings could be determined as shown in expanded region of the spectrum (Fig. 6B).

For establishing the robustness of the sequence CH-DQSERF experiments were also carried out on the molecules **1** and **3**. The methyl group selective CH-DQSERF spectra of **1** and **3** are reported in Figs. 7A and 8A, respectively. Analogous to previously discussed molecule, for these molecules also the spin system is A_3X in t_1 dimension and the resulting spectrum is a doublet of doublet. For the molecule **2**, the doublet separations d and k reported in Fig. 7B corresponds to $2(^{2}T_{HH})$ for *R* and *S*, respectively. On the other hand the spin system in the direct dimension is A_3MX. The SQ cross-section for each double quantum transition in t_1 dimension is a doublet of a triplet and thus represents the 1D spectrum of methyl group displaying $^{2}T_{HH}$ and $^{3}T_{HH}$ couplings. Similarly for molecule 3, the spin system in t_2 dimension is A_3MNPX. Thus the

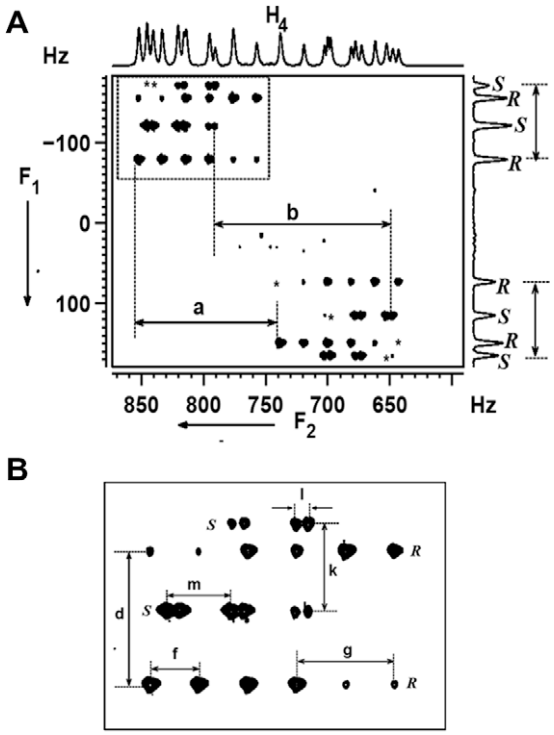

Fig. 7. (A) 500 MHz ^{1}H 2D CH-DQSERF spectrum of **1** in the chiral liquid crystal PBLG correlating the DQ coherence of methyl protons to its SQ coherence along with the corresponding projections. All the peaks of 2D projection in the direct dimension could be correlated to the peaks in *R* and *S* enantiomer cross-sections; (B) The expanded part of the spectrum marked in (A) marked with broken rectangle. Peak separations providing the values (in Hz) are: $a = (^{1}T_{CH})^{R} = 113.0$, $d = 2(^{3}T_{HH})^{R} = 64.4$, $g = (^{2}T_{HH})^{R} = 37.2$, $f = (^{3}T_{HH})^{R} = 19.3$; $b = (^{1}T_{CH})^{S} = 142.0$, $k = 2(^{2}T_{HH})^{S} = 44.6$, $m = (^{2}T_{HH})^{S} = 22.3$ and $l = (^{3}T_{HH})^{S} = 6.2$.

spectrum is enantiopure for the methyl group in each cross-section and displays the coupling parameters as reported in the figure captions. The coupling parameters derived by the analyses of all these spectra are reported in the corresponding figure captions.

2.5. Advantages and limitations of the techniques

There are several advantages of CH-SERF and CH-DQSERF experiments, viz., (a) there is a complete separation of the overlapped spectra of methyl peaks for each enantiomer in both direct and indirect dimensions, (b) both passive homo and heteronuclear couplings could be derived from the indirect dimension in both the experiments, (c) the reduced multiplicity in the DQ dimension of the CH-DQSERF experiment enhanced the resolution of the spectra and enabled unambiguous visualization, (d) the cross-section taken along SQ dimension at each transition in the DQ dimension provided all the active couplings, (e) invoking additional coupling parameter, $^{1}T_{CH}$, resulted in better chiral discrimination and enabled the determination of the couplings which were not possible in the DQSERF experiment due to poor resolution, (f) when one of the experiments do not provide all the information due to loss of resolution, the combined use of CH-SERF and CH-DQSERF aided the analyses, (g) as far as the sensitivity is concerned, it is similar to any inverse experiments where the polarization transfer is through INEPT sequence and (h) the experimental pulse sequence is simple, robust and easy to implement.

The proposed experiments also suffer from certain limitations. The spin systems must be weakly coupled for selective excitation in both sequences. Therefore the sequences cannot be applied to strongly coupled spin systems where the selective excitation is not possible. The resonances of the coupled spins must be well iso-

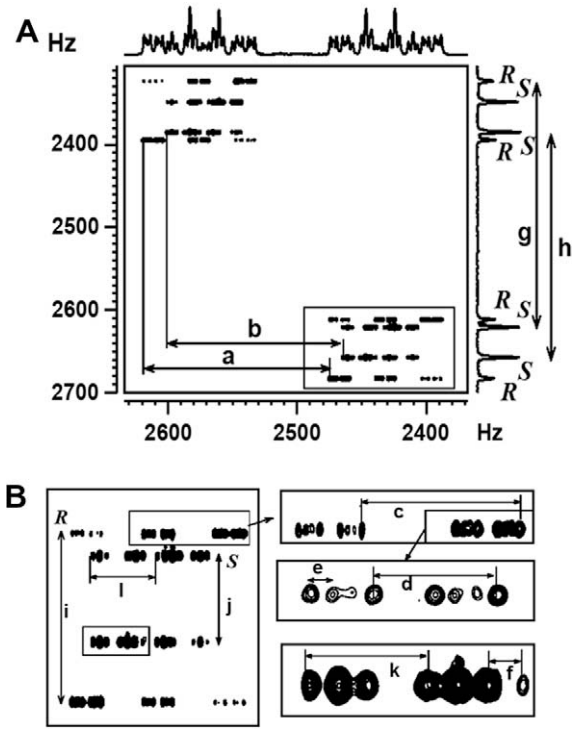

Fig. 8. (A) 500 MHz ^{1}H 2D CH-DQSERF spectrum of **3** in the chiral liquid crystal PBLG correlating the DQ coherence of methyl protons to its SQ coherence along with the corresponding projections. All the peaks of 2D projection in the direct dimension could be correlated to the peaks in *R* and *S* enantiomer cross-sections; (B) The expanded part of the spectrum marked with rectangle in (A). Peak separations providing the couplings and their values in Hz are: a = $(^{1}T_{CH})^{R}$ = 144.0, i = $2(^{2}T_{HH})^{R}$ = 72.2, c = $(^{2}T_{HH})^{R}$ = 36.1, d = $(^{3}T_{HH})^{R}$ = 13.7 and e = $(^{4}T_{HH})^{R}$ = 4.8; b = $(^{1}T_{CH})^{S}$ = 136.0, j = $2(^{2}T_{HH})^{S}$ = 36.4, l = $(^{2}T_{HH})^{S}$ = 18.2, k = $(^{3}T_{HH})^{S}$ = 9.8 and f = $(^{4}T_{HH})^{S}$ = 4.5.

lated, especially the methyl group for CH-DQSERF experiment. It may be pointed out that during INEPT transfer both $^{1}T_{CH}$ and $^{2}T_{HH}$ evolve with differential values for *R* and *S* enantiomers and the transfer of magnetization is not uniform for a chosen τ delay. Thus the proposed sequences cannot be employed for the precise measure of enantiomeric excess. Furthermore, during the t_1 period the signal is both cosine and sine modulated. Hence the 2D Fourier transform will give absorptive and dispersive components which cannot be phased. Thus the spectra are processed in magnitude mode.

3. Conclusions

The two experimental methodologies for unambiguous chiral discrimination have been developed. The experiments also provided the short and long distance couplings. The problem of overlap of central transitions in the selective methyl protons excited SERF has been overcome. The CH-DQSERF experiment resulted in larger dispersion of the spectra in the indirect dimension and enabled better chiral discrimination. The cross-section taken along the SQ dimension at each transition in the DQ dimension provided all the active couplings. The combined use of CD-DQSERF and the judicious choice of selective excitations in CH-SERF enable the determination of all the spectral parameters.

Acknowledgments

N.N. thanks UGC, India for Junior research fellowship and Mr. Sankeerth Hebbar and Mr. Uday Ramesh Prabhu for helpful discussions. N.S. gratefully acknowledges the financial support by Department of Science and Technology, New Delhi for the Grant No. SR/S1/PC-32/2008.

Appendix A. Supplementary data

Supplementary data associated with this article can be found, in the online version, at doi:10.1016/j.jmr.2009.06.011.

References

[1] C. Aroulanda, M. Sarfati, J. Courtieu, P. Lesot, Investigation of the enantioselectivity of three polypeptides liquid crystal solvents using NMR spectroscopy, Enantiomer 6 (2001) 281–287.
[2] A.S. Tracey, The orientations of molecules dissolved in lyotropic surfactant solutions, Mol. Phys. 33 (2001) 339–350.
[3] K. Kobzar, H. Kessler, B. Luy, Stretched gelatin gels as chiral alignment media for the discrimination of enantiomers by NMR spectroscopy, Angew. Chem. Int. Ed. 44 (2005) 3145–3147.
[4] R. Montecinos, H. Ahumada, R. Martinez, F.A. Olea, R. Araya-Maturana, M.P. Aliste, D.P. Tieleman, B.E. Weiss-López, Structure and aggregation number of a lyotropic liquid crystal: a fluorescence quenching and molecular dynamics study, Langmuir 20 (2004) 5703–5708.
[5] J.M. Péchiné, A. Meddour, J. Courtieu, Monitoring the differential ordering of enantiomers included into cyclodextrins through deuterium NMR in lyotropic liquid crystals, Chem. Commun. (2002) 1734–1735.
[6] U. Eliav, G. Navon, Collagen fibers as a chiral agent: a demonstration of stereochemistry effects, J. Am. Chem. Soc. 128 (2006) 15956–15957.
[7] P. Lesot, D. Merlet, J. Courtieu, J.W. Emsley, T.T. Rantala, J. Jokisaari, Calculation of the molecular ordering parameters of (±)-3-Butyn-2-ol dissolved in an organic solution of poly(γ-benzyl-L-glutamate), J. Phys. Chem. A 101 (1997) 5719–5724.
[8] P. Lesot, O. Lafon, J. Courtieu, P. Berdagué, Analysis of the ^{13}C NMR spectra of molecules, chiral by isotopic substitution, dissolved in a chiral oriented environment: towards the absolute assignment of the pro-*R*/pro-*S* character of enantiotopic ligands in prochiral molecules, Chem. Eur. J. 10 (2004) 3741–3746.
[9] V.M. Marathias, G.J. Tawa, I. Goljer, A.C. Bach II, Stereochemical identification of (*R*)- and (*S*)-Ibuprofen using residual dipolar couplings, NMR, and modeling, Chirality 19 (2007) 741–750.
[10] S.P. Sau, K.V. Ramanathan, Visualization of enantiomers in the liquid-crystalline phase of a fragmented DNA solution, J. Phys. Chem. B 113 (2009) 1530–1532.
[11] I. Canet, J. Courtieu, A. Loewenstein, A. Meddour, J.M. Péchiné, Enantiomeric analysis in a polypeptide lyotropic liquid crystal by deuterium NMR, J. Am. Chem. Soc. 117 (1995) 6520–6526.
[12] P. Lesot, M. Sarfati, J. Courtieu, Natural abundance deuterium NMR spectroscopy in polypeptide liquid crystals as a new and incisive means for the enantiodifferentiation of chiral hydrocarbons, Chem. Eur. J. 9 (2003) 1724–1745.
[13] D. Merlet, M. Sarfati, B. Ancian, J. Courtieu, P. Lesot, Description of natural abundance deuterium 2D-NMR experiments in weakly ordered liquid-crystalline solvents using a tailored Cartesian spin-operator formalism, Phys. Chem. Chem. Phys. 2 (2000) 2283–2290.
[14] P. Lesot, D. Merlet, A. Loewenstein, J. Courtieu, Enantiomeric visualization using proton-decoupled natural abundance deuterium NMR in poly(γ-benzyl-L-glutamate) in liquid crystalline solutions, Tetrahedron Asymmetry 9 (1998) 1871–1881.
[15] D. Merlet, W. Smadja, J. Courtieu, P. Lesot, B. Ancian, Analysis of natural abundance deuterium NMR spectra of enantiomers in chiral liquid crystals via 2D auto-correlation experiments, Chem. Commun. (1998) 2301–2302.
[16] O. Lafon, P. Lesot, D. Merlet, J. Courtieu, Modified z-gradient filtering as a mean to obtain phased deuterium autocorrelation 2D NMR spectra in oriented solvents, J. Magn. Reson. 171 (2004) 135–142.
[17] O. Lafon, P. Lesot, Deuterium 3D NMR experiments for analysing weakly aligned, isotopically enriched solutes, Chem. Phys. Lett. 404 (2005) 90–94.
[18] P. Lesot, O. Lafon, Enantiomeric analysis using natural abundance deuterium 3D NMR spectroscopy in polypeptide chiral oriented media, Chem. Phys. Lett. 458 (2008) 219–222.
[19] A. Meddour, P. Berdague, A. Hedli, J. Courtieu, P. Lesot, Proton-decoupled carbon-13 NMR spectroscopy in a lyotropic chiral nematic solvent as an analytical tool for the measurement of thee Excess, J. Am. Chem. Soc. 119 (1997) 4502–4508.
[20] P. Lesot, J. Courtieu, Natural abundance deuterium NMR spectroscopy: developments and analytical applications in liquids, liquid crystals and solid phases, Prog. Nucl. Magn. Reson. Spectrosc. (2009). doi:10.1016/j.pnmrs.2009.01.001.
[21] J. Farjon, L. Ziani, L. Beguin, D. Merlet, J. Courtieu, Selective NMR excitations in chiral analysis, Ann. Rep. NMR Spectrosc. 61 (2007) 283–293.
[22] N. Giraud, M. Joos, J. Courtieu, D. Merlet, Application of a ^{1}H δ-resolved 2D NMR experiment to the visualization of enantiomers in chiral environment, using sample spatial encoding and selective echoes, Magn. Reson. Chem. 47 (2009) 300–306.

[23] B. Bikash, R.P. Uday, N. Suryaprakash, Enantiomeric discrimination by double quantum excited selective refocusing (DQ-SERF) experiment, J. Phys. Chem. B 111 (2007) 12403–12410.
[24] B. Bikash, R.P. Uday, N. Suryaprakash, Binuclear spin state selective detection of ^{1}H single quantum transitions using triple quantum coherence: a novel method for enantiomeric discrimination, J. Magn. Reson. 192 (2008) 92–100.
[25] B. Bikash, R.P. Uday, N. Suryaprakash, Spin state selective coherence transfer: a method for discrimination and complete analyses of the overlapped and unresolved ^{1}H NMR spectra of enantiomers, J. Magn. Reson. 192 (2008) 101–111.
[26] R.P. Uday, B. Bikash, N. Suryaprakash, Separation and complete analyses of the overlapped and unresolved ^{1}H NMR spectra of enantiomers by spin selected correlation experiments, J. Phys. Chem. A 112 (2008) 5658–5669.
[27] R.P. Uday, N. Suryaprakash, Band selective small flip angle COSY: a simple experiment for the analyses of ^{1}H NMR spectra of small chiral molecules, J. Magn. Reson. 195 (2008) 145–152.
[28] V.M. Marathias, I. Goljer, A.C. Bach II, Simultaneous determination of ^{1}H–^{1}H and ^{1}H–^{13}C residual dipolar couplings in a chiral liquid crystal solvent using a natural abundance HSQC experiment, Magn. Reson. Chem. 43 (2005) 512–519.
[29] J. Farjon, D. Merlet, P. Lesot, J. Courtieu, Enantiomeric excess measurements in weakly oriented chiral liquid crystal solvents through 2D ^{1}H selective refocusing experiments, J. Magn. Reson. 158 (2002) 169–172.
[30] J. Farjon, J.-P. Baltaze, P. Lesot, D. Merlet, J. Courtieu, Heteronuclear selective refocusing 2D NMR experiments for the spectral analysis of enantiomers in chiral oriented solvents, Magn. Reson. Chem. 42 (2004) 594–599.
[31] T. Fäcke, S. Berger, SERF, a new method for H, H spin-coupling measurement in organic chemistry, J. Magn. Reson. A 113 (1995) 114–116.
[32] G.A. Morris, R. Freeman, Enhancement of nuclear magnetic resonance signals by polarization transfer, J. Am. Chem. Soc. 101 (1979) 760–762.
[33] L. Ziani, J. Courtieu, D. Merlet, Visualisation of enantiomers via insertion of a BIRD module in X–H correlation experiments in chiral liquid crystal solvent, J. Magn. Reson. 183 (2006) 60–67.
[34] D. Merlet, B. Ancian, J. Courtieu, P. Lesot, Two-dimensional deuterium NMR spectroscopy of chiral molecules oriented in a polypeptide liquid crystal: applications for the enantiomeric analysis through natural abundance deuterium NMR, J. Am. Chem. Soc. 121 (1999) 5249–5258.
[35] J. Keeler, Understanding NMR Spectroscopy, John Wiley and Sons, England, 2005.